Reprint from

PLASMA PHYSICS AND CONTROLLED NUCLEAR FUSION RESEARCH 1988

PROCEEDINGS OF THE
TWELFTH INTERNATIONAL CONFERENCE ON PLASMA PHYSICS
AND CONTROLLED NUCLEAR FUSION RESEARCH
HELD BY THE
INTERNATIONAL ATOMIC ENERGY AGENCY
IN NICE, 12-19 OCTOBER 1988

In three volumes

VOLUME 2

INTERNATIONAL ATOMIC ENERGY AGENCY
VIENNA, 1989

NON-LINEAR MHD STUDIES IN TOROIDAL GEOMETRY — DISRUPTIVE PHENOMENA IN TOKAMAK PLASMAS*

A.Y. AYDEMIR, R.D. HAZELTINE, M. KOTSCHENREUTHER,
J.D. MEISS, P.J. MORRISON, D.W. ROSS, F.L. WAELBROECK,
J.C. WILEY
Institute for Fusion Studies,
The University of Texas at Austin,
Austin, Texas

R.E. DENTON[1], J.F. DRAKE, R.G. KLEVA
Laboratory for Plasma and Fusion Energy Studies,
University of Maryland,
College Park, Maryland

United States of America

Abstract

NON-LINEAR MHD STUDIES IN TOROIDAL GEOMETRY — DISRUPTIVE PHENOMENA IN TOKAMAK PLASMAS.

Sawtooth oscillations and related fluid excitations are studied analytically and computationally, and some modifications relevant to high temperature regimes are presented. — The role of the ideal kink in the sawtooth crash and a new theory of density limit disruptions are discussed.

1. NONLINEAR MHD STUDIES IN TOROIDAL GEOMETRY

A. Y. Aydemir, R. D. Hazeltine, M. Kotschenreuther,
J. D. Meiss, P. J. Morrison, D. W. Ross, F. L. Waelbroeck,
and J. C. Wiley

Sawtooth oscillations and related fluid excitations are studied analytically and computationally, and some modifications relevant to high temperature regimes are discussed.

1.1 Toroidal Studies of Sawtooth Oscillations

Tokamak sawtooth oscillations are studied computationally with a nonreduced, fully toroidal, resistive MHD (magnetohydrodynamic) model that includes ohmic heating and parallel and perpendicular thermal conduction.

We examine the effects of transport on the type of sawtooth oscillations using simple models for the perpendicular heat transport coefficient, $\kappa_\perp$. With a constant $\kappa_\perp$, simple, periodic sawtooth oscillations are seen (Fig. 1a). When the time evolution of $\kappa_\perp$ is coupled to the dynamics by letting $\kappa_\perp \sim p^{-1/2}$,

---

* Supported by the US Department of Energy.

[1] Present address: Institute for Fusion Studies, The University of Texas at Austin, TX 78712, USA.

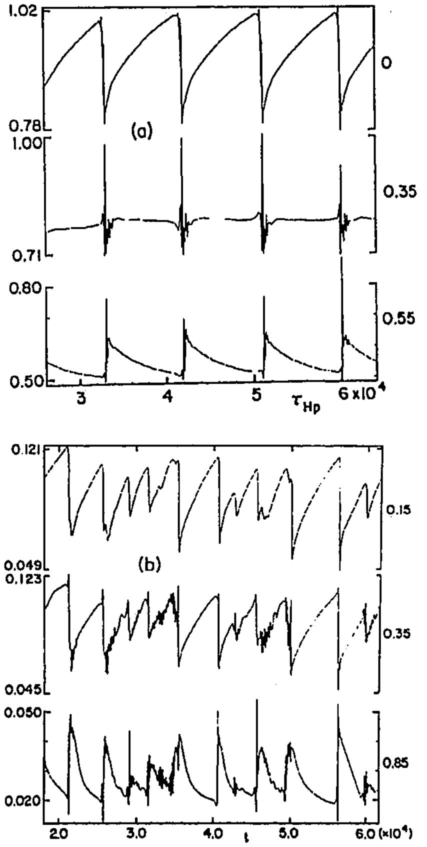

FIG. 1. (a) Computational soft X-ray signals for the simple sawtooth oscillations produced when a constant-$\kappa_\perp$ model is used. The top figure is from the central channel, the middle one through the inversion radius, and the bottom one from a channel outside the inversion radius. (b) Computational ECE (local temperature) measurements for a set of complex sawteeth obtained when $\kappa_\perp \sim p^{-1/2}$. Top figure: magnetic axis, middle figure: further out along the major radius, but within the inversion radius, bottom: outside the inversion radius. Times are normalized to the poloidal Alfvén time, τ_{Hp}. Data are rotated with a period of 250 τ_{Hp}.

where p is the pressure, we observe more complex sawtooth behavior involving giant sawteeth with temperature modulations of order unity, interspersed with smaller oscillations, some of which exhibit multiple partial relaxations (Fig. 1b). Note that the density is assumed to be constant in our model. Thus, the terms pressure and temperature will be used interchangeably in this section. We observe that the off-axis minima in the $q-$ profile (cause of compound sawteeth) is not necessarily associated with a hollow temperature profile, but that it can result from a contraction of the plasma column due to large heat flux to the wall when $\kappa_\perp \sim p^{-1/2}$, thus large near the wall.

In order to explain the crash times of $\sim 100\mu\text{sec}$, an ideal, pressure driven (quasi-interchange) mode was proposed as the crash mechanism [1]. Linear and nonlinear studies [2,3] of these modes in weak shear equilibria have indicated that they may in fact be responsible for some of the recent experimental observations from large tokamaks. However, in our self-consistent studies where the sawtooth oscillations are followed on a transport time scale, we find the role played by the ideal quasi-interchange mode to be insignificant. During the sawtooth ramp, we observe a brief period during which the ideal mode is active. However, the weak shear q–profile with $q \gtrsim 1$ in the central region is modified by ohmic heating such that, first, we see $q \lesssim 1$ in the center, which converts the ideal mode into a resistive interchange, with a similar eigenfunction but with a growth rate that is now a function of the resistivity. Then, as q_o continues to drop below one, the weak shear conditions are lost, with $q_o \lesssim 0.9$, and the mode becomes a resistive kink. The sawtooth crash is thus caused not by an ideal quasi-interchange mode, but by a resistive kink, the growth rate of which is seen to scale as $\gamma \sim S^{-1/3}$.

These results were obtained with $S \lesssim 2 \times 10^6$. For large tokamaks, $S \geq 10^8$. Thus, at realistic values of S, the disparity between the transport time-scale, the time scale on which the q–profile changes, and the growth time of the

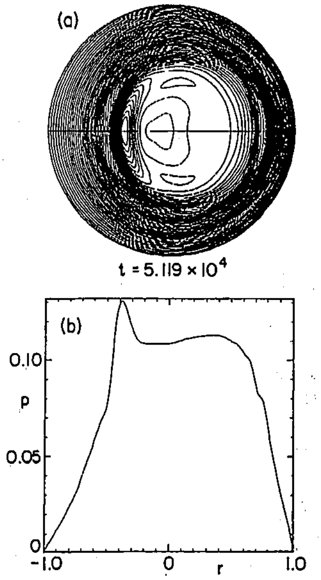

FIG. 2. (a) Pressure contours towards the end of a typical simple crash, showing a crescent shaped high pressure(temperature) region that was previously associated only with quasi-interchange modes; (b) pressure along the midplane.

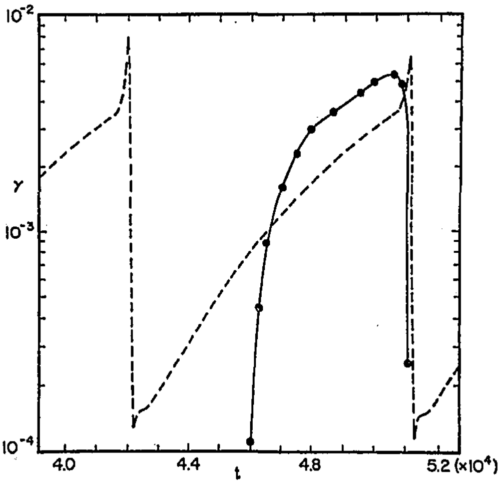

FIG. 3. Linear growth rate of n = 1 mode during simple sawtooth period. Soft X-ray signal from the central chord for this period is also shown (dashed line).

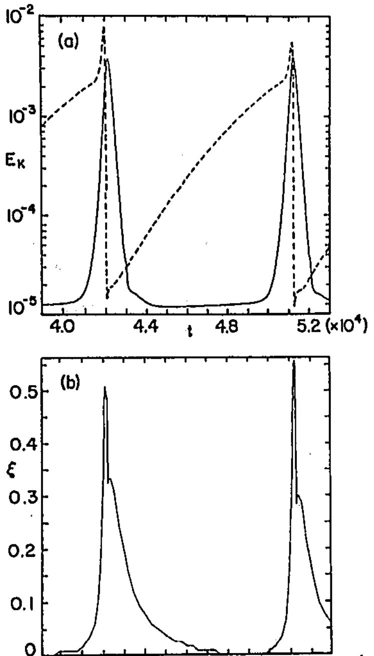

FIG. 4. (a) Evolution of total kinetic energy in the system during sawtooth period of Fig. 3; (b) displacement of pressure peak during crash. Only the portions with $d\xi/dt > 0$ are meaningful. Note that the unstable period in Fig. 3 is much longer than these gross diagnostics would indicate.

ideal mode is enhanced. Thus, one might expect an ideal quasi-interchange-driven crash under more realistic conditions where the mode has sufficient time to grow. However, without significant flux reconnection, that scenario seems unlikely, as earlier studies have found this mode to saturate in a helical equilibrium [2,3]. Although the displacement of the core away from the center during this helical shift may be interpreted as a sawtooth crash, eventual poloidal symmetry observed experimentally after the crash was never seen in those studies.

Our scaling studies with the resistive kink mode, however, yield promising, if not conclusive, results. Extrapolating from results obtained with $S \in [2 \times 10^4 - 2 \times 10^6]$, we get crash times of $500 - 1000\mu$sec for $S = 10^8$. Although slower than experimental observations, this result does not rule out the Kadomtsev reconnection process as the cause of the fast crashes. Our studies are continuing in this area, and further exploration with different transport models may indeed give crash times of $\lesssim 100\mu$sec.

X-ray tomography studies from JET [4] indicate a cold "bubble" formation during the crash that is partially surrounded by a hot crescent shaped region. This was contrasted with the cold, crescent shaped island of the Kadomtsev model, and in order to explain this presumed anomaly, again the quasi- interchange mode was invoked [1]. Indeed, nonlinear studies [2,3] did find close agreement between the nonlinear phase of this mode and the bubble observations from JET. However, we find that a hot crescent is formed during the crash even with resistive kink modes (Fig. 2). This topological feature is found to be a finite-β effect that results from the hot core being displaced violently towards the $q = 1$ surface, where it gets deformed into the observed semi-circular region partially enclosing a cold "bubble". Thus, we do not see an inconsistency between this feature of the JET crashes and the Kadomtsev model.

An important issue in the recent literature has been the sudden transition from the sawtooth ramp to the crash. This fast trigger has been previously interpreted to imply that the mode causing the crash has to be "turned on" in a time shorter than the crash time τ_c itself. This point is also contradicted by our studies. We see an unstable mode growing for a substantial portion of the sawtooth period (Fig. 3). The crash represents the final stages of the nonlinear evolution of the mode, the resistive kink in our case, and occurs quite a long time ($\gtrsim 10\tau_c$) after the mode goes unstable. During most of the period when the mode is growing, it is not detected by gross diagnostics such as island width, the total kinetic energy, or the displacement of the temperature peak. In fact, observations of these quantities would erroneously lead one to believe that the crash is caused by a mode triggered only a brief period ($\sim \tau_c$) before the crash (Fig. 4). The fast trigger is a result of the hot core being displaced rapidly by a mode that has gone through many e-folding periods, not by a mode that suddenly goes unstable. Admittedly, this argument does not quantitatively explain the trigger problem. However, it indicates that

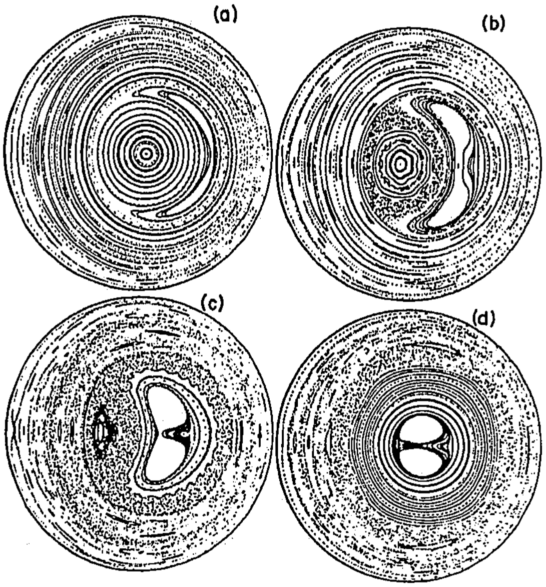

FIG. 5. Field line plots during a crash (simple sawteeth): (a) at the top of the crash; (b, c) during the crash, and (d) at the bottom of the crash.

correlating the trigger with a mode that is switched on in a period of $\sim \tau_c$ is incorrect.

For the plasma β considered here (toroidal $\beta \simeq 2\%, \epsilon\beta_p \simeq 0.1$), the crash is followed by a compressional wave that propagates out to the wall; thus, it is felt almost simultaneously at all radii. The crash represents a significant perturbation to the plasma column. Flattening of the pressure and current density profiles in the center modifies the global MHD equilibrium, and the column readjusts itself to establish a new equilibrium. The pulse that propagates outward from the inversion radius represents this adjustment. The effects of this ballistic wave on the diffusive portion of the heat pulse and thermal diffusivity, χ_{Hp}, measurements need to be investigated further.

The helical shift in the pressure profile, which starts the crash, is accompanied by the growth of an $m = 1$ island. The evolution of the island and development and healing of stochastic field lines are shown in Fig. 5. At the top of the crash, Fig. 5a, and further down the crash in Fig. 5b, islands of different helicities are present. In addition to the large $m = 1$ island, one can easily identify $(m, n) = (2, 1), (3, 2)$, and $(5, 2)$ primary island chains. Note also the formation of secondary island chains inside the $q = 1$ surface. As the crash proceeds, interaction of the secondary islands leads to a large band of stochastic region around the island separatrix (Fig. 5c). The development of this stochastic layer, however, does not prevent full reconnection. Stochastic regions develop also outside the inversion radius, around the separatrices of other primary islands such as $(m,n) = (2,1),(3,2)$, and $(4,3)$, as seen in Fig. 5c, and at the bottom of the crash in Fig. 5d. However, these tend to stay as bands separated by good flux surfaces, since the primary islands never become large enough for complete island overlap. After the crash, the stochastic regions gradually shrink and good flux surfaces form again.

1.2 Analytic Studies of the Quasi-Interchange Mode

Simulations of the entire sawtooth cycle reveal that the quasi-interchange begins growing relatively early during the ramp phase of the sawtooth oscillations, but is not the direct cause of the crash. The failure of this instability to cause a disruption shortly after the onset of growth can be attributed to its nonlinear saturation. We have studied these effects analytically by generalizing the dispersion relation found previously for the ideal quasi-interchange [5,6].

The free energy liberated by the 1/1 interchange results in a positive Δ' at the $q = 2$ surface. The interchange driving forces enter Δ' through the coefficient σ given linearly by [7]

$$\sigma_{lin} = \int_0^{a/r_2} \frac{(\epsilon\beta_p)^2}{(1-1/q)^2}\rho^5 d\rho \tag{1}$$

At finite amplitude, this term is found to be reduced from its linear value by an amplitude dependent correction: $\sigma = \sigma_{lin} - \Lambda\xi^2$. We have calculated Λ for two model current profiles: a constant current profile bounded by a current sheet, and a gaussian profile of $1 - 1/q$. Both cases yielded positive values of Λ, resulting in saturation of the tearing mode growth.

1.3 Kinetic Modifications

The resistive MHD results for tearing mode behavior are significantly modified by kinetic effects in the present generation of high temperature toroidal confinement devices. We find that neoclassical rotation damping from toroidicity often stabilizes $m = 1$ tearing modes. This offers an explanation for the experimental measurements of $q < 1$ in steady state, which implies that reconnecting tearing modes have been suppressed. For $m = 1$ modes, the mode frequency ω is typically satisfies $\nu > \omega \gg \nu\,(B_p/B)^2$ with ν the poloidal rotation damping rate. Using previously derived neoclassical equations [8], we obtain the following normalized linearized equations for flux ψ, potential ϕ, and pressure p. All times and distances are normalized to the classical $m = 1$ tearing mode growth time γ_c^{-1} and mode width x_L :

$$-i\,(\omega - \omega_{*i})\left(1 + I + \frac{i\nu}{\omega}\right)\frac{d^2\phi}{dx^2} + ix\frac{d^2\psi}{dx^2} \;=\; 0 \tag{2}$$

$$-i\left(\omega-\omega_{*e}\right)\psi+ix(\phi-p) \;=\; \frac{d^2\psi}{dx^2} \qquad (3)$$

$$\omega p=\omega_*\phi+xf\frac{d^2\psi}{dx^2} \qquad (4)$$

where ω_{*e} and ω_{*i} are the electron and ion diamagnetic frequencies; nonzero $f=\left(\rho_i/x_L\right)^2$ gives semicollisional effects, where ρ_i is the ion gyroradius. The first equation is the vorticity equation with neoclassical damping and inertial enhancement [9] $I \sim \epsilon^{-3/2}$; the second equation is Ohm's Law with parallel pressure gradients, and the last equation is the pressure evolution equation. Bootstrap current effects are small here, as are parallel sound flows for these frequencies.

Equations (2-4) can be solved analytically for $f = 0$; for $T_e = T_i$ the mode stability criterion in unnormalized units is $\omega_*^2\nu > \gamma_c^3$. In the banana regime, $\nu \sim \nu_{ii}\epsilon^{-3/2}$; surprisingly, this then is an electron beta criterion $\beta_e > 0.4\epsilon^{-7/4}(dq/dr)(d\ln p/dr)^{-1}$. For realistic profiles, this is $\beta_e > .002-.003$.

Numerical solution of Eqs (2)–(4) has been carried out for finite f and for finite Δ' (which arises from toroidicity). Semicollisional effects (f) reduce the stabilizing effects of rotation damping, but the mode is still often stable for many machines, particularly near reactor parameters. However, the layer width can become smaller than an ion banana width; then Eqs (2)–(4) are not valid. The ions become adiabatic, damping effects are reduced, and semicollisional kinetic effects dominate. In the semicollisional regime, new terms arise from including a radial electric field and adiabatic-ion induced electrostatic potentials. A nonlinear analysis indicates that even in this regime there can be a strong barrier to island growth for island widths less than the banana width.

2. DISRUPTIVE PHENOMENA IN TOKAMAK PLASMAS

R. E. DENTON , J. F. DRAKE, and R. G. KLEVA

The role of the ideal kink in the sawtooth crash and a new theory of density limit disruptions are discussed.

2.1 The Role of the Ideal Kink in the Sawtooth Crash

In order to study the role of the ideal kink mode in causing the sawtooth crash, we have derived a set of low beta toroidal reduced MHD equations. These are derived through an expansion in $\epsilon(=a/R)$, and will be presented in a future publication. Corrections to the vorticity equation are retained to two orders higher than that required in a cylinder, while elsewhere only one higher order is retained. The equations have been incorporated into our 3-D sawtooth code. They include finite pressure, however we will only present results at zero beta.

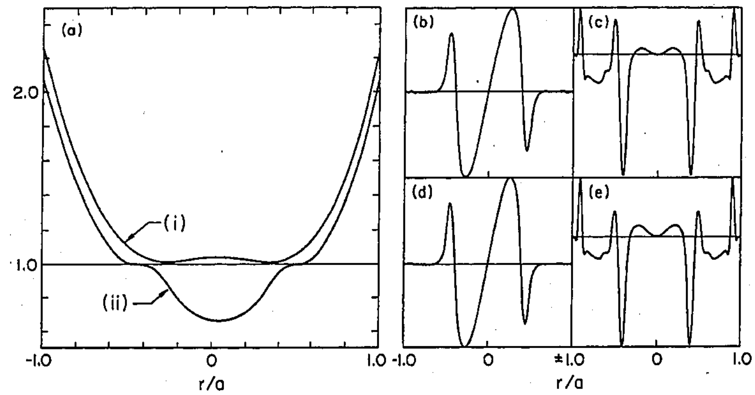

FIG. 6. (a) Profiles of safety factor q; (b,c) profiles of m/n = 1/1 and 2/1 toroidal current for linear non-monotonic q ideal kink with Δq = 0.2 and ε = 0.1 using the full MHD code; (d, e) same profiles using toroidal reduced MHD code.

If the q profile is nonmonotonic [with $q_{\rm min}$ off axis as in Fig. 6a(i)] and $q_{\rm min} \geq 1$, then the ideal kink mode is unstable in toroidal geometry even at zero β [10]. In a test case using both the full MHD code [2] and the reduced MHD code for $\Delta q = q_0 - q_{\rm min} = 0.2$ and $q_{\rm min} = 1.0$ with $\epsilon = 0.1$, the linear growth rates agreed to within 5% and the linear eigenmodes (Fig. 6b–d) were in good agreement.

Nonmonotonic q profiles can arise naturally if the temperature profile is flat or hollow or if $z_{\rm eff}$ is peaked [11]. It has been speculated that ideal sawtooth crashes might result from such q-profiles as $q_{\rm min}$ drops toward one from above due to thermal instability [10]. We will examine the possible role of this mode in causing the sawtooth crash over a range of resistivities $\eta (= 1/S)$ down to $\eta = 2.5 \times 10^{-7}$.

When we run the reduced MHD code nonlinearly at $\eta = 10^{-5}$ starting with a q profile with a very large $\Delta q = 0.2$ at $\epsilon = 0.25$, the $n = 1$ ideal kink displaces the plasma to one side on a fast time-scale, $\sim 100\tau_A$. The temperature only symmetrizes as q slowly flattens and falls below one on a resistive time scale. However, when we start with profiles evolved self-consistently in one of our cylindrical runs [11] having $\Delta q = 0.03$ with $q_{\rm min} > 1$ [Fig. 6a(i)], and run it at $\epsilon = 0.25$, an ideal displacement does not occur at $\eta = 10^{-5}$, nor at $\eta = 2.5 \times 10^{-6}$. As q falls, the ideal mode does become unstable; however, before it can grow to large amplitude, q falls below one and the ideal mode becomes stable. As q continues to drop, resistive reconnection results and the persistent sawteeth are Kadomtsev-like. When the central temperature is plotted versus time, the sawteeth appear more rounded than in a cylinder and they have larger precursor oscillations, apparently due to a reduced tearing mode growth rate in a torus at zero β. Thus, the ideal kink is not important for resistivities down to $\eta = 2.5 \times 10^{-6}$.

At lower resistivity, an ideal displacement can occur. The rate at which q falls goes like η, and lower η gives the mode more time to grow before q drops below one. Time dependent temperature traces at radius $r/a = 0.29$ and the kinetic energy growth rate are displayed in Figs 7a,b for a run with $\eta = 2.5 \times 10^{-7}$. As $q_{\min}$ dropped, the $m/n = 1/1$ mode, somewhat localized to the $q = 1$ surface, became unstable. But as the mode grew nonlinearly, the $m/n = 2/2$ mode and then the 3/3 mode dominated even though the linear 1/1 growth rate was the largest. A 3/3 saturation occurred with three cold spots bulging in toward the center, but leaving the central temperature relatively unaffected (Fig. 7c), and this pattern persisted.

Efforts are under way to run with lower η. Since the $n = 1$ mode goes unstable at a higher value of $q_{\min}$ than the $n > 1$ modes, the $n = 1$ mode may dominate at lower η. In considering the relationship of these results to the sawtooth crash, many questions remain, such as what is the time-scale of the displacement at lower η, how can a displacement lead to a crash of the central temperature, and how does q evolve after a crash.

In order to study the behavior of discharges with q-profiles like those measured on TEXTOR [12], we have also run cases with $q_0 = 0.7$ at $\epsilon = 0.25$. Parabolic q-profiles were found to reconnect resistively all the way to the center at values of η as low as 2.5×10^{-7}. We have found that by flattening the q-profile [12], we can obtain linear stability to the $n = 1$ resistive mode for a fixed q-profile [Fig. 6a(ii)]. However, when we evolved this case nonlinearly, the flat q-region fell below one and magnetic reconnection began at the $q = 1$ surface and eventually raised q above one everywhere.

2.2 Density Limit Disruptions

An increase in the line averaged plasma density $\bar{n}$ beyond a critical value $\bar{n}_c \sim B_\phi/q_a R$ in tokamak discharges leads to violent MHD activity, a rapid loss of energy confinement and the abrupt termination of the discharge. It has

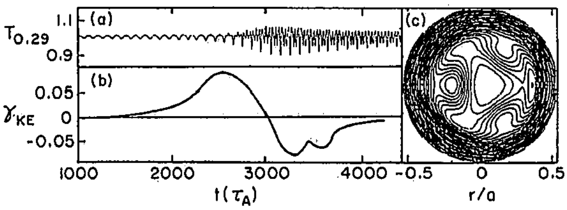

FIG. 7. (a, b) Time dependent traces of $T_{0.29}$, temperature at r/a = 0.29 and γ_{KE}, kinetic energy growth rate for run described in text with $\eta = 2.5 \times 10^{-7}$; (c) temperature contours at $t = 4400\ \tau_A$.

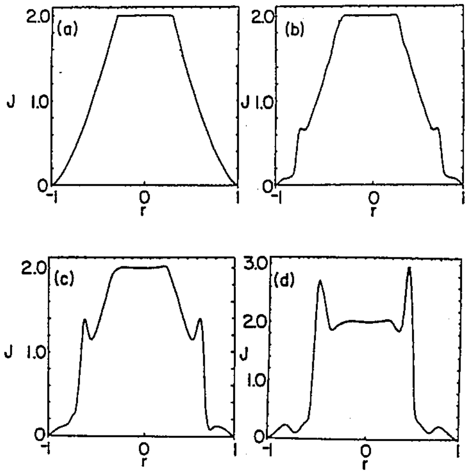

FIG. 8. Current profiles during rise in edge radiation.

been recognized for a number of years that line radiation from the cold edge plasma plays a role in triggering the disruption, yet the mechanism by which a benignly sawtoothing discharge abruptly evolves from a stable to a violently unstable configuration has remained a mystery.

The relative stability of sawtoothing tokamak discharges is now well understood. In MHD simulations of such discharges the $q = 2$ mode and other helicities remain either stable or saturate at small amplitudes. Two important characteristics of these discharges account for their stability. First, current profiles with q flat and near one across the center resemble a top hat current distribution with $q = 1$ inside the plasma, which is marginally stable to all tearing modes and external kinks [13]. Secondly, when $q(r = 0) \sim 1$, the large difference in the pitch of the magnetic field between the $q = 2$ surface and central plasma prevents the $q = 2$ mode from growing to large amplitude even if it is linearly unstable [14]. A complete model of density limit disruptions must therefore explain how line radiation from the edge plasma can cause the abrupt transition away from the stable sawtoothing current profile and how the magnetic shear between $q = 2$ surface and the central plasma can be reduced (on a short time scale) so that the $q = 2$ mode can grow to large amplitude. We present such a model.

We have completed simulations of density limit disruptions by incorporating a simple model for line radiation into the temperature equation of our 3-D resistive MHD code:

$$\frac{dT}{dt} - \nabla_\perp \cdot \kappa_\perp \nabla \perp T - \kappa_{||}(\mathrm{B} \cdot \nabla)^2 T = \Omega \eta J^2 - L \qquad (5)$$

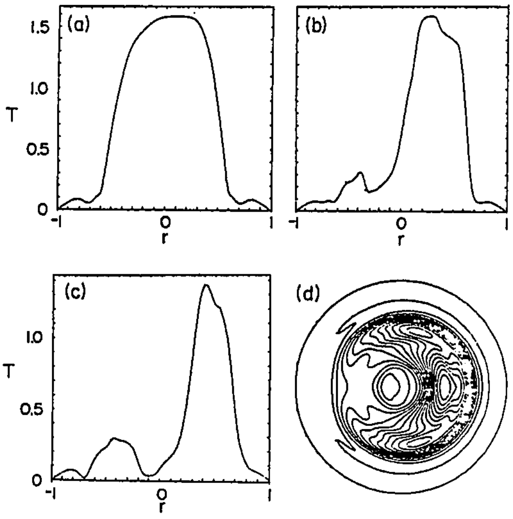

FIG. 9. Bubble injection during m = 1 kink mode.

The radiation function L is chosen to model line radiation from the low temperature edge plasma; it is nonzero over the temperature range $T_{\mathrm{min}} < T < T_{\mathrm{max}}$, with an increasing amplitude to model the rising plasma density. A description of the code, which is based on the reduced MHD equations, has been presented previously [14]. In the present simulations the electric field at the wall is adjusted to maintain a constant total current. The resistivity is evolved self-consistently with the temperature using the classical relationship $\eta \sim T^{-3/2}$. All of the computations presented were run at $\eta \sim 10^{-5}$.

The results in Fig. 8 show the effect of rising edge radiation on a typical current profile in a sawtoothing discharge $[q(0) \sim 1]$. As the radiation increases, the edge temperature drops and the current which had been flowing in the edge region is forced inward, producing a pronounced skin current. As the current profile contracts, this skin current becomes larger and moves up the gradient, successively destabilizing modes which are rational at progressively decreasing values of q (e.g., 2/1, 3/2, 4/3, ...). While the magnetic islands associated with these modes can grow to moderate size, the islands die away without affecting central confinement as the current profile continues to contract. Ultimately, the skin current rises to the top of the current gradient causing the minimum value of q to fall below one off axis. This current profile is unstable to a $q = 1$ kink, which convects a bubble of cold, radiating edge plasma into the center of the plasma column (Figs 9a-c). The bubble can be clearly seen in the plot of temperature contours shown in Fig. 9d (same time as Fig. 9c) and is similar to the bubble which is seen in tomographic analyses of density limit disruptions on JET [15].

The formation of the bubble is insensitive to the resistivity of the central plasma since the reconnection occurs in the outer cold plasma region and not in the hot plasma. Skin current profiles with $q(0) \sim 1$, which form just prior to the bubble injection, are similar to those studied in connection with the evolution of the ideal $q = 1$ kink [16] and the sawtooth crash [17]. In both cases, a cold plasma bubble is injected into the central plasma on a time-scale independent of the resistivity of the hot plasma.

The entire formation of the bubble can be calculated analytically in the following idealized model. As the plasma density increases in a sawtoothing discharge with $q(0) \sim 1$ and total current I, the edge radiation cools the edge plasma, forcing the original current profile (solid line in Fig. 10a) to contract and form a current profile (dashed line in Fig. 10a) with a skin current at r_0. The magnitude of the skin current is equal to the current I_0 which originally flowed in the region $r > r_0$. The q-profile produced by this skin current (dashed line in Fig. 10b) has an off-axis minimum at r_0 with a value $q_{\min} = 1 - I_0/I$. The $q = 1$ rational surface lies in the region of cold plasma at $r_1 = r_0/q_{\min}^{1/2}$. This skin current profile is unstable to a $q = 1$ mode which reconnects the reversed $q = 1$ helical flux in the cold plasma region $r_0 < r < r_2$, where r_2 is given by $r_2^2/r_0^2 - 1 = (2/q_{\min}) \ln(r_2/r_0)$. Following reconnection, the cold magnetic island shrinks to a bubble of radius r_b and is injected into the central plasma. Plasma incompressibility requires that $r_b^2 = r_2^2 - r_0^2$. The q profile following injection of the bubble is shown by the dotted line in Fig. 10b. Since the current flowing in the cold plasma bubble is low, $q(0)$ is very large. Conservation of flux in the hot plasma requires that a positive skin current form at r_b and a negative skin current at r_2. The hot plasma occupies the ring $r_b < r < r_2$ where $q = 1$. The negative skin current is rapidly dissipated by the cold edge plasma, while the total current is conserved, producing the q-profile given by the solid curve in Fig. 10b. The bubble radius r_b increases rapidly with the skin current I_0. The maximum possible bubble radius $r_b = r_1$

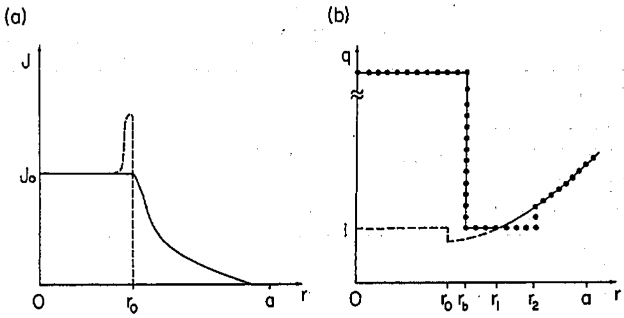

FIG. 10. Current profiles (a) and q-profiles (b) before and following bubble injection.

is reached when the fraction of the current outside the sawtoothing region $I_0/I = (e-2)/(e-1) = .42$, where $e = 2.718$.

The first phase of the disruption is completed with the injection of the cold plasma bubble. The second phase of the disruption begins as a broad spectrum of modes grows on the double valued q-profile produced by the bubble. These modes progressively raise the minimum value of q by reconnecting the flux across the hot plasma annulus: the 6/5 mode raises q_{min} from 1.0 to 1.2, the 5/4 mode from 1.2 to 1.25, etc., until the 3/2 mode raises q_{min} above 1.5. At this point the magnetic shear between the $q = 2$ surface and the plasma center has been greatly reduced and the $q = 2$ mode reconnects across the entire central plasma, raising q above 2 everywhere and throwing the remaining hot plasma to the wall. The final growth of the $q = 2$ mode is insensitive to the central plasma resistivity since the flux reconnection occurs primarily in the region of cold plasma [18].

REFERENCES

[1] WESSON, J.A., Plasma Phys. Control. Fusion **28** (1986) 243.

[2] AYDEMIR, A.Y., Phys. Rev. Lett. **59** (1987) 649.

[3] HOLMES, J.A., CARRERAS, B.A., CHARLTON, L.A., LYNCH, V.E., HASTIE, R.J., HENDER, T.C., Phys. Fluids **31** (1988) 1202.

[4] EDWARDS, A.W., et al., Phys. Rev. Lett. **57** (1986) 210.

[5] HASTIE, R.J., HENDER, T.C., Nucl. Fusion **28** (1988) 585.

[6] WAELBROECK, F.J., HAZELTINE, R.D., Phys. Fluids **31** (1988) 1217.

[7] WAELBROECK, F.L., Non-Linear Growth of the Quasi-Interchange Instability, IFSR 331, Institute for Fusion Studies Report (July 1988), submitted to Phys. Fluids.

[8] KOTSCHENREUTHER, M., et al., in Plasma Physics and Controlled Nuclear Fusion Research 1986 (Proc. 10th Int. Conf. Kyoto, 1986), Vol. 2, IAEA, Vienna (1987) 249.

[9] SHAING, K.C., HIRSCHMAN, S.P., Bull. Am. Phys. Soc. **31** (1986) 1495.

[10] BUSSAC, M.N., LERBINGER, K., PELLAT, R., TAGGER, M., in Plasma Physcis and Controlled Nuclear Fusion Research 1986 (Proc. 10th Int. Conf. Kyoto, 1986), Vol. 2, IAEA, Vienna (1987) 17; HASTIE, R.J., HENDER, T.C., CARRERAS, B.A., CHARLTON, L.A., HOLMES, J.A., Phys. Fluids **30** (1987) 1756.

[11] DENTON, R.E., DRAKE, J.F., KLEVA, R.G., BOYD, D.A., Phys. Rev. Lett. **56** (1986) 2477.

[12] SOLTWISCH, H., STODIEK, J., MANICKAM, J., SCHLÜTER, J., in Plasma Physics and Controlled Nuclear Fusion Research 1986 (Proc. 10th Int. Conf. Kyoto, 1986), Vol. 1, IAEA, Vienna (1987) 263.

[13] SHAFRANOV, V.D., Zh. Tekh. Fiz. **40** (1970) 241.

[14] DRAKE, J.F., KLEVA, R.G., Phys. Rev. Lett. **53** (1984) 1465.

[15] CAMPBELL, D.J., et al., in Plasma Physics and Controlled Nuclear Fusion Research 1986 (Proc. 10th Int. Conf. Kyoto, 1986), Vol. 2, IAEA, Vienna (1987) 433.

[16] ROSENBLUTH, M.N., MONTICELLO, D.A., STRAUSS, H.R., WHITE, R.B., Phys. Fluids **19** (1976) 1987.

[17] KLEVA, R.G., DRAKE, J.F., DENTON, R.E., Phys. Fluids **30** (1987) 2119.

[18] KLEVA, R.G., DRAKE, J.F., DENTON, R.E., MHD Simulation of Density Limit Disruptions in Tokamaks (to be published).

Printed by the IAEA in Austria